Mycobacterium tuberculosis cords within lymphatic endothelial cells to evade host immunity.

Thomas R. Lerner[1,6], Christophe J. Queval[1,6], Rachel P. Lai[2], Matthew Russell[3], Antony Fearns[1], Daniel J. Greenwood[1], Lucy Collinson[3], Robert J. Wilkinson[2,4,5], and Maximiliano G. Gutierrez[1*]

[1]Host-pathogen interactions in tuberculosis laboratory, [2]Tuberculosis laboratory, [3]Electron Microscopy Scientific Technology Platform, The Francis Crick Institute, 1 Midland Road, London, NW1 1AT, UK; [4]Wellcome Centre for Infectious Diseases Research in Africa, Institute of Infectious Disease and Molecular Medicine, and Department of Medicine, University of Cape Town, Cape Town 7925, Republic of South Africa; [5]Department of Medicine, Imperial College London, London W2 1PG, United Kingdom. [6] These authors contributed equally to the work.

[*]Corresponding author: Maximiliano G. Gutierrez. The Francis Crick Institute, 1 Midland Road London NW1 1AT United Kingdom
Telephone: +44 (0) 203 796 1460
E-mail: max.g@crick.ac.uk

Abstract

The ability of *Mycobacterium tuberculosis* to form serpentine cords is intrinsically related to its virulence, but specifically how *M. tuberculosis* cording contributes to pathogenesis remains obscure. We show that several *M. tuberculosis* clinical isolates form intracellular cords in primary human lymphatic endothelial cells (hLEC) in vitro and also in the lymph nodes of patients with tuberculosis. We identified via RNA-seq a transcriptional programme that activates, in infected-hLECs, cell-survival and cytosolic surveillance of pathogens pathways. Consistent with this, cytosolic access is required for intracellular *M. tuberculosis* cording. Mycobacteria lacking ESX-1 type VII secretion system or PDIM expression, which fail to access to the cytosol, are indeed unable to cords within hLECs. Finally, we show that *M. tuberculosis* cording is a size-dependent mechanism used by the pathogen to avoid its recognition by cytosolic sensors and evade either resting or IFN-γ-induced hLEC immunity. These results explain the long-standing association between *M. tuberculosis* cording and virulence and how virulent mycobacteria use intracellular cording as strategy to successfully adapt and persist in the lymphatic tracts.

Introduction

Mycobacterium tuberculosis is one of the deadliest bacterial pathogen of humankind and still constitutes a global health challenge (1). A striking phenotype of *M. tuberculosis* growing in nutrient broth is the ability of this pathogen to form serpentine cords, a morphological observation originally described by Robert Koch (2). This cording phenotype is intimately associated with virulence and immune evasion (3). The first morphological descriptions of *M. tuberculosis* growth in liquid and solid media described a distinct ability of tubercle bacilli to form large and elongated structures by Middlebrook, Dubos and Pierce in the mid-1940s (4). Cording is a complex phenotype involving many mycobacterial factors including lipids such as the "cord-factor" glycolipid trehalose dimycolate (TDM) (5-7) and a series of chemical modifications such as cyclopropanation of mycolic acids in the cell wall (3).

Similar cording has been reported in other pathogenic mycobacteria, primarily in liquid media or extracellularly in various cell and organism models of infection. In zebrafish, *M. abscessus* released from apoptotic macrophages grows extracellularly, forming cords (8). It is postulated that apoptosis of infected macrophages is a key event in the release of bacteria within the extracellular space and subsequent initiation of cord formation. There are, however, few reports showing that cording can also occur intracellularly. In 1928, Maximow and co-workers first reported intracellular cording in tissue culture (9). In 1957, Shepherd studied this phenomenon in HeLa cells and found that only fully virulent *M. tuberculosis* strains formed cords (10). More recently, Ferrer and co-workers showed that an attenuated mutant of *M. tuberculosis* formed cords in fibroblasts (11).

Overall, extracellular cording has been shown in mycobacteria to be anti-phagocytic and to be a trigger of extracellular trap formation in macrophages (8, 12, 13). Although proposed as a virulence mechanism, this does not explain why an intracellular pathogen such as *M. tuberculosis* would prefer to replicate in cords in the relatively nutrient poor extracellular space to avoid phagocytosis.

Bacterial xenophagy is the process that regulates the removal of cytosolic bacteria after damage to phagosomal membranes during selective macroautophagy (14). This pathway constitutes one of the first cell autonomous defence pathways against intracellular pathogens (15, 16). A fraction of the *M. tuberculosis* population damage phagosomes to access the cytosol and are subsequently recognised by autophagic adaptors and the xenophagy machinery. This process targets *M. tuberculosis* into autophagosomes and thus the lysosomal

degradation pathway (17). Whereas there is a large body of literature demonstrating autophagy as an anti-mycobacterial pathway (18), recent evidence shows that *M. tuberculosis* can eventually block the fusion of autophagosomes with lysosomes (19, 20) and in mice, *M. tuberculosis* can evade autophagic responses in vivo (21).

Pulmonary tuberculosis is the most common form of the disease but lymphatics and lymph nodes are almost systematically involved (22). Recent reports proposed that lymphatics may contribute to disease systemic dissemination and persistence (23, 24). *M. tuberculosis* mostly infects macrophages although there is compelling evidence that a minor proportion of *M. tuberculosis* is found infecting various non-myeloid cells in the lungs and lymph nodes in vivo (25-28). The role that these *M. tuberculosis* subpopulations play in TB pathogenesis in different cell types (e.g. immune vs non-immune) is unclear. We previously showed in extrapulmonary tuberculosis that a subpopulation of *M. tuberculosis* is found in human lymphatic endothelial cells (hLEC) in lymph node biopsies and these cells could represent a reservoir for *M. tuberculosis* in infected patients (19).

Here we discovered that *M. tuberculosis* forms large intracellular cords consisting of up to thousands of individual bacteria arranged end-to-end, in hLEC and in biopsies of tuberculosis patients. This intracellular cording phenotype is a common feature to virulent *M. tuberculosis* clinical isolates from the 4 human adapted strain lineages (1 to 4), while attenuated strains, lacking functional type VII secretion system or either Phthiocerol dimycocerosates (PDIM) production, failed to form intracellular cords. We analysed by RNAseq the host-environment during *M. tuberculosis* challenge and identified a transcriptional signature, from *M. tuberculosis*-infected hLECs, consistent with membrane damage and bacterial escape from the phagosome into the cytosol. We use correlative light electron microscopy (CLEM) to determine that intracellular cords are formed of chains of individual *M. tuberculosis*, which are only present in the host cell cytosol, suggesting that cytosolic access is a pre-requisite for intracellular bacterial cording. *M. tuberculosis* mutants lacking ESX-1 or PDIMs, that cannot access the cytosol, are indeed incapable of cording unless co-cultured with wild-type bacteria to 'smuggle' them from a shared phagosome into the cytosol. We finally, show that cords are devoid of endosomal, phagosomal and autophagosomal cellular markers and are formed from bacteria that successfully evaded p62-dependent xenophagy. Our results argue that intracellular cording represents an immune evasion strategy selected by virulent mycobacteria to survive within hLECs. When growing, the bacteria-forming cords, too large

to be recognised by cytosolic sensors, represents a size-dependent mechanism that *M. tuberculosis* use to avoid it recognition and clearance by host degradative pathways such as xenophagy.

Results

M. tuberculosis forms extensive intracellular cords in hLECs and lymph node biopsies

By monitoring GFP-expressing *M. tuberculosis* H37Rv (GFP-*M. tuberculosis*) replication in hLECs at different time points after infection, we observed a striking ability of *M. tuberculosis* to form distinctive intracellular cords over the time (**Figure 1A**). 3D confocal imaging of *M. tuberculosis*-infected hLECs for 72 hours, confirmed these cords to be intracellular rather than on the cell surface (**Figure 1B**). To quantitatively and accurately measure intracellular *M. tuberculosis* cording, we used the maximum Feret diameter, representing the distance between the two furthest extremities of the cord (**Supplemental Figure 1**). As expected from **Figure 1A**, *M. tuberculosis* intracellular cords rapidly expend over time, reaching sizeable Feret diameters up to 150 μm only 72 h post-infection (**Figure 1C**). Intracellular cording was also observed in a human type II alveolar epithelial cell line (A549) although less prominent than in hLEC, likely due to the A549 cells themselves being smaller than hLEC (**Figure 1D**). Intracellular cord formation was present not only in the lab-adapted strain H37Rv (Lineage 4) but also when hLEC were infected with any of the three clinical isolates, N0072, N0145, N0024, representing *M. tuberculosis* lineages 1, 2 and 3, respectively (**Figure 1E**). Importantly, the cords were also present in lymph nodes of extrapulmonary TB patients (**Figure 1F**). We indeed observed that in Ziehl-Neelsen-stained lymph nodes with TB granulomas, intracellular bacterial cords were present in cells with pleiotropic morphologies, including endothelial-like morphology (**Figure 1F**). To confirm these observations, sections were stained for the lymphatic endothelial marker podoplanin (PDPN) and *M. tuberculosis* (19). Despite only few LEC are infected with *M. tuberculosis*, the intracellular cording phenotype was associated with LEC in lymph node biopsies and the size of these cords ranged from 4 to 21 μm (**Figure 1F**). Thus, the ability of *M. tuberculosis* to cord intracellularly in vitro in primary hLECs is not only conserved among the virulent human-adapted mycobacteria, but is also clinically relevant.

158 ***M. tuberculosis* infection induces cytosolic surveillance of bacterial pathogens and pro-**
159 **survival response in hLECs**
160 To better understand the host cell response to the extensive *M. tuberculosis* cording in the
161 cytosol, we performed RNA-seq analysis in uninfected and *M. tuberculosis*-infected hLEC at
162 48 h after infection when cords started to be prominent. Among the top ten statistically
163 significant process networks induced by *M. tuberculosis* infection, we found group of genes
164 related to inflammation and interferon signalling, phagosome and antigen presentation and
165 innate immune response (**Figure 2A**). In addition to a strong pro-inflammatory response, we
166 identified additional pathways that were significantly up-regulated after infection including
167 cytosolic RNA and dsDNA sensing with an upregulation of type I interferon (**Figure 2B**). The
168 pathways of cytosolic carbohydrate recognition as well as STING signalling were also
169 upregulated suggesting a high level of membrane damage induced by *M. tuberculosis* (**Figure**
170 **2B**). Importantly, RNA-seq identified a transcriptional signature consistent with pro-survival
171 pathways and antigen presentation (**Figure 2C**). This pro-survival signature was unexpected
172 based on our data on human primary macrophages (29), although consistent with previous
173 live-cell observations that active *M. tuberculosis* replication in primary hLECs was not
174 associated with significant host cell death (19). We then confirmed by RT-qPCR the mRNA
175 expression of the pro-inflammatory cytokine *IL-6* as well as the type I IFN responsive cytokines
176 *CXCL10* (IP10) and *IFNB1* after infection in hLECs (**Figure 2D**). The pro-survival factors *BCL2A1*,
177 *EIF2AK2* and *TNFAIP3* (A20), the cytosolic glycan sensing genes Galectin-3 (L*GALS3*), Galectin-
178 8 (*LGALS8*), *cGAS* and the foreign DNA sensor *ZBP1* were also significantly up-regulated after
179 infection (**Figure 2D**). In the case of *LGALS3*, a high level of expression was observed already
180 in uninfected cells (**Figure 2D**). Thus, infection of hLECs with *M. tuberculosis* induced host pro-
181 survival pathways and negative regulators of cell death to protect the niche in which bacteria
182 proliferate. On the other hand, endothelial cells upregulated cytosolic surveillance of RNA,
183 DNA and carbohydrates pathways to recognise *M. tuberculosis* in the cytosol.
184
185 ***M. tuberculosis* intracellular cords are localised in the cytosol**
186 Given that the significant upregulation of cytosolic pathogen surveillance during cording in
187 hLECs, we next sought to define the subcellular compartment within which *M. tuberculosis*
188 cords. By using a correlative imaging approach (correlative light and electron microscopy,
189 CLEM), we determined that *M. tuberculosis* intracellular cords were localised in the cytosol of

hLEC in long structures that (in this example) looped around the host cell nucleus (**Figure 3A**). In contrast, small groups of *M. tuberculosis* containing relatively low numbers of individual bacteria were localised in a membrane-bound compartment (**Figure 3B**) as reported before (19). The cords are usually formed of a bundle of several parallel chains of *M. tuberculosis* (**Figure 3C**) and therefore a single cord can consist of (up to) thousands of individual bacteria. We then measured by three-dimensional serial block face (3D SBF) CLEM the volume of 25 individual bacteria (displayed as coloured reconstructions) contained in a cord (**Figure 3C**) or in the membrane bound small-clump (**Figure 3D**). Interestingly, the volume of bacteria forming a cord was significantly lower than the non-cording bacteria (**Figure 3E**). This confirmed that the cords did not consist of abnormally long and filamentous mycobacteria, but is more likely formed by actively replicating bacteria. We concluded that *M. tuberculosis* intracellular cording occurs in the cytosol of hLEC and that cytosolic *M. tuberculosis* cords are composed of hundreds or thousands of individual mycobacteria that are smaller than bacteria contained in membrane-bound compartments.

***M. tuberculosis* lacking RD1 locus or PDIMs expression fail to cord within hLECs**

We next sought to understand *M. tuberculosis* factors that contributed to the intracellular cording phenotype in hLEC. We have previously shown that the ESX-1 secretion system, encoded in the RD1 genomic region, and the cell wall lipid PDIMs are required for intracellular replication of *M. tuberculosis* in hLEC (19, 30) as well as in macrophages (31-33). Infection with the *M. tuberculosis* ΔRD1 mutant that lacks the ESX-1 secretion system was not able to form cords but instead exhibited smaller clumps of bacteria sometimes with a mesh-like appearance (**Figure 4A**). Similarly, the phenotype of the *M. tuberculosis* mutant lacking PDIM (ΔPDIM) (31) also presented a clumpy mesh-like phenotype with an increased number of individual bacteria that were not organised in cords (**Figure 4A**). As shown **Figure 1C**, the Feret diameter of intracellular RFP-*M. tuberculosis* wild-type (WT) increased over the time, while the size of both E2 Crimson-ΔRD1 or GFP-ΔPDIM mutants remain significantly lower than wild-type (WT) strain even after 3 days of infection (**Figure 4B**). Importantly, the lack of cording observed with the ΔRD1 mutant was not due to the reduced bacterial burden, since increasing the multiplicity of infection did not increase cord formation although significant bacterial growth was observed (**Figure 4C-F**). Moreover, we found that the up-regulation of some genes in hLEC after infection (**Figure 2B**) such as interferon-beta (*IFNB1*) or interleukin-

6 (*IL-6*) was RD1 and PDIM dependent (**Supplemental Figure 2**). For other genes, ESX-1 and PDIM seem to play a suppressive role, suggesting that other *Mtb* factors are involved in the activation of immune pathways. Altogether, these results confirm that intracellular cording in hLEC is specific to virulent *M. tuberculosis* strains. Attenuated *M. tuberculosis* strains, lacking functional ESX-1 secretion system or PDIMs, are indeed unable to cord within cells. Interestingly, it is known that both deletion of RD1 locus or inhibition of PDIM expression affect the ability of mycobacteria to escape from phagosome to reach the cytosol. Together with the exclusive cytosolic localisation of virulent *M. tuberculosis* cords (shown **Figure 3**), the inability of those attenuated mutant to cord, suggest that bacterial access to the cytosol may be required for the cording.

Access to the cytosol is required for *M. tuberculosis* replication and intracellular cording

The localisation of *M. tuberculosis* cords suggested that the cytosol represents a permissive environment for *M. tuberculosis* replication, thus we tested if the ΔRD1 mutant of *M. tuberculosis* that is mostly localised in membrane-bound compartments could replicate and form intracellular cords if forced to access the cytosol. To achieve that, we performed a series of co-infection experiments combined with CLEM. As shown before, in RFP-*M. tuberculosis* H37Rv WT single infection of hLEC, RFP-*M. tuberculosis* WT formed prominent intracellular cords whereas single infection with E2-Crimson-*M. tuberculosis* ΔRD1 or GFP-*M. tuberculosis* ΔPDIM did not show cording (**Figure 5A**). Strikingly, if hLEC are co-infected with RFP-*M. tuberculosis* WT and with E2-Crimson-*M. tuberculosis* ΔRD1 or GFP-*M. tuberculosis* ΔPDIM, the *M. tuberculosis* mutants lacking either ESX1 or PDIM were now able to clearly form intracellular cords (**Figure 5A**). Consistent with these observations, co-infection with *M. tuberculosis* WT partially restored the ability of ΔRD1 or ΔPDIM mutants to cord (**Figure 5B**). Whereas lower than the WT, the Feret diameter of both E2-Crimson-*M. tuberculosis* ΔRD1 or GFP-*M. tuberculosis* ΔPDIM in co-infected cells was significantly increased compare to the single infection condition (**Figure 5B**). Importantly, in co-infected cells, both the *M. tuberculosis* ΔRD1 or ΔPDIM were able to replicate more efficiently (**Figure 5C**). By CLEM, we confirmed that the RFP-*M. tuberculosis* WT was localised in the cytosol and defined at the ultrastructural level that the cords formed by GFP-*M. tuberculosis* ΔRD1 in co-infected cells were now localised in the cytosol (**Figure 5D and E**). Altogether our data demonstrate that forcing the access to the cytosol of attenuated ΔRD1 or ΔPDIM mutants by co-infection with

M. tuberculosis WT strain, restore both their intracellular replication and their ability to cords intracellularly. This confirms that the effect of ESX-1 or PDIM expression on intracellular cording is mediated by access to the cytosol.

Intracellular cords are not recognized by cytosolic immune sensors in both resting or IFN-γ-activated hLECs.

Bacterial access to the cytosol is essential for the replication of virulent mycobacteria, which when exposed to the cytosolic components, must avoid being recapture by host-immune sensors and targeted for degradation. In hLEC, *M. tuberculosis* targeting via selective autophagy is PDIM dependent (30) and entirely RD1 dependent (**Supplemental Figure 2**) suggesting that in hLECs, xenophagy primarily recognises mycobacteria that access the cytosol. As cytosolic location is a pre-requisite for mycobacterial cording in hLECs, we hypothesized that bacterial cords originate from bacteria, which successfully evade host-degradative pathways such as xenophagy. We thus examine both the dynamic of intracellular bacterial growth and its association with the autophagic marker p62 (**Figure 6A-C**, **Supplemental Movies 1-3**). Live cell imaging of *M. tuberculosis*-infected hLECs expressing RFP-p62 revealed that the intracellular cords form from bacteria which have either completely evaded p62-positive compartments (**Figure 6A and Supplemental Movie S1**) or which have initially been growth-restricted in a p62-positive state (**Figure 6B**) but subsequently became p62-negative, where this process can also cycles several times (**Figure 6C and Supplemental Movie 2**). Crucially, the *M. tuberculosis* cords only ever form once the bacteria lost p62 (**Figure 6C and Supplemental Movie 3**) suggesting that cording is a consequence of avoiding an autophagic state or that cord formation blocks autophagic targeting, potentially by being too large to encapsulate and recapture from the cytosol. Thus, we investigated whether cording vs non-cording populations of *M. tuberculosis* present in hLECs 72 h.pi were differentially recognised by the selective autophagy machinery. When we co-labelled ubiquitin and p62 in cord-containing cells, we notably found that both markers selectively associated with mostly small bacterial clusters but not with *M. tuberculosis* cords, as defined by having a Feret diameter greater than 10 µm (**Figure 6D** and **E**). Importantly, large *M. tuberculosis* cords, neither associated with selective autophagy markers Galectin-8, NDP52 and LC3B as well as the late endosomal/lysosomal markers LAMP-2 and cathepsin D, while single or small groups/clumps of bacteria (Feret diameter < 10 µm) presented a higher

association with all those markers (**Figure 6E**). These data indicated that cytosolic *M. tuberculosis* cords were not recognised by xenophagy or any other immune sensor tested.

We previously reported that in resting hLECs, autophagy is not necessarily detrimental for virulent mycobacteria but when activated with IFNG prior to infection; the autophagy pathway restricted bacterial growth and promoted bacterial clearance (19). We then examine whether intracellular cords still evade cytosolic detection by autophagy machinery in IFNG-activated hLECs. As observed in resting hLECs, mostly small bacterial clusters were targeted by autophagic markers LC3B and p62, while intracellular cords were not recognized by any of them (**Figure 6F and G**). Those data confirm that intracellular cording is an effective mechanism use used by virulent mycobacteria to evade hLECs immune defences and to persist within lymphatic endothelium.

Discussion

Since the identification of *M. tuberculosis* as the etiologic agent of human TB, the phenomenon of cording has attracted significant interest because of its association with virulence and infection in vivo. Whereas there are many studies that implicate extracellular cording as a mechanism to subvert phagocytosis, there is little evidence regarding the role of intracellular cords in *M. tuberculosis* pathogenesis. We show here that *M. tuberculosis* intracellular cords are a size-dependent mechanism of evasion of endothelial host cell intracellular innate immune defences such as xenophagy. We postulate that cords are linked to virulence because bacteria can replicate to a large extent intracellularly within non-immune cells in a protected environment until nutrients are exhausted and space to grow is limited. Mycobacteria are then released into the extracellular milieu where large cords can block phagocytic uptake, allowing dissemination of *M. tuberculosis*. This is similar to the extracellular cords that form in the *M. absessus* infected zebrafish model where cords are too large to be phagocytosed and therefore facilitate immune evasion (8). We determined that intracellular cording is a result of evading the host cell defences and allows vast numbers of bacteria to proliferate, only being stopped by physical space and eventually leading to the cell being compromised and cords disseminating, which are too large for phagocytosis by macrophages and/or neutrophils**.**

High burdens of cytosolic bacteria without induction of host cell death was surprising and suggested that human endothelial cells respond differently to infection that in human primary

318 macrophages (29)**.** Several pathological studies have shown that while some bacilli produce
319 massive tissue damage, especially in the lung, others persist in many tissues with no gross
320 evidence of damage (34). We propose that infection in macrophages tends to induce necrotic
321 cell death whereas endothelial cells are more resistant to cell death and permissive for *M.*
322 *tuberculosis* growth. Consistent with the prolonged survival of *M. tuberculosis*-infected hLEC,
323 there is an *M. tuberculosis*-induced transcriptional signature of cell death present but this is
324 alongside the upregulation of several pro-survival pathways. Our studies are consistent with
325 early observations in HeLa cells that found that only fully virulent *M. tuberculosis* strains could
326 cord, often filling the whole cell without causing cytotoxicity (10). Finally, our data provide an
327 explanation for the observation that endothelial cells are infected in patients with
328 tuberculosis but the typical clinical symptoms of endothelial damage are not observed as in
329 other infectious diseases.
330 Our study also sheds some light on the preferred site of replication of *M. tuberculosis* in
331 endothelial cells. Our experiments clearly show that if bacteria access the cytosol, they can
332 cord and replicate. This suggests that the environment in membrane bound compartments is
333 restrictive and the cytosol highly permissive for bacterial replication and cording. It remains
334 to be defined if that is the case for macrophages. Interestingly, in one study that investigated
335 the localisation of *M. tuberculosis* in resected lungs of tuberculosis patients, prominent cords
336 were observable within macrophages at the luminal side of the granuloma cavity (35). If our
337 studies in human cells and tissue are reflected in mice remains to be determined, however,
338 the evasion of xenophagy by intracellular cording might provide an explanation for the
339 reported evasion of this pathway in the mouse model of tuberculosis (21).
340 What determines that a subpopulation of intracellular *M. tuberculosis* starts cording? It is
341 possible that differential expression of *M. tuberculosis* secreted or cell-surface proteins cause
342 differential recognition of cytosolic *M. tuberculosis* by the autophagy apparatus. Modification
343 affecting the synthesis of bacteria wall component such as trehalose dimycolate (TDM) is
344 important for cording in vitro and bacterial virulence in vivo (3, 36). Here, we observed that
345 individual bacteria forming intracellular cords were smaller than membrane-bound non-
346 cording bacteria, suggesting that the localization of those two bacterial populations may differ
347 at the transcriptional level. We can speculate that the lower volume of individual bacteria
348 forming intracellular cords is the results of modification in the bacterial wall composition,
349 improving the ability of bacteria to form cords within hLEC cytosol and modulate the

recognition by cytosolic sensors. Our data show that the previously reported ubiquitin-mediated autophagy process by which *M. tuberculosis* extracellular DNA/RNA is recognised by the cGAS/STING pathway (17) is also activated in hLEC. Whether it is the bacteria themselves that are ubiquitinated or their compartment is uncertain. If *M. tuberculosis* retains its waxy cell wall in the cytosol it is unlikely that ubiquitination will play a major role in xenophagic targeting. We reason that if the bacteria themselves are being recognised, then why is only a subpopulation targeted to autophagy? What is different about them? We hypothesise that it is the ESX-1 mediated damaged membranes surrounding bacteria that are recognised, and if *M. tuberculosis* is in close proximity to this it will be 'captured' with it. This process may be cyclical, with *M. tuberculosis* then damaging the autophagic compartment to escape again. However, if *M. tuberculosis* can get away from the damaged membranes after cytosolic translocation, it may be able to evade autophagic capture. This is likely to occur for the majority of the *M. tuberculosis*, hence why only a relatively small population are targeted to autophagy. It is unlikely that dead bacteria or those that do not damage the phagosomal membrane will be targeted to autophagy because it is ESX-1 and PDIM dependent; these populations are thus likely to mature into phagolysosomes. Although the cording phenotype seems to be unique for pathogenic mycobacteria, it remains to be determined if other cytosolic pathogens also evades autophagy in a size-dependent manner as shown here.

Methods

Cells

Primary hLEC taken from inguinal lymph nodes (ScienCell Research Laboratories, #2500) were cultured according to the manufacturer's instructions up to passage 5 as described fully in (19). For confocal microscopy of fixed cells, 20,000 cells in 300 µl complete endothelial cell medium (ECM) (ScienCell Research Laboratories, #1001) were seeded onto 10 mm diameter #1.5 glass coverslips (Glaswarenfabrik Karl Hecht, #1001/10_15). For imaging destined for CLEM, 10,000 cells per dish (MatTek, #P35G-1.5-14-CGRD) in 500 µl ECM were seeded to achieve a confluence of 30-50% (thus allowing visualisation of the grid reference etched into the dish). For live cell imaging, 25,000 cells per dish in 500 µl ECM were seeded to achieve a confluence of >80% (thus limiting the cells' movement away from the field of view). For electron microscopy, 200,000 cells per T25 flask were seeded in 5 ml ECM. For imaging with the automated confocal microscope Opera Phenix, 5,000 cells per well were seeded in 96 well

plate (Cell Carrier 96 ultra, PerkinElmer). Type II alveolar epithelial A549 cells (ATCC) were cultured according to the manufacturer's instructions. For confocal microscopy, 50,000 cells in 500 µl DMEM (Gibco) supplemented with 10% (v/v) heat inactivated foetal calf serum (FCS) were seeded onto 10 mm diameter #1.5 glass coverslips.

***Mycobacterium tuberculosis* strains**

This study used the following EGFP tagged strains as described previously (19, 30, 31): *Mycobacterium tuberculosis* H37Rv-EGFP (*M. tuberculosis* WT), *M. tuberculosis* H37Rv-EGFP ΔRD1 (*M. tuberculosis* ΔRD1). In this study, we refer to the *M. tuberculosis*-GFP WT strain as *M. tuberculosis* WT, the *M. tuberculosis*-GFP PMM100 strain as *M. tuberculosis* ΔPDIM. Additionally, we have used M. tuberculosis H37Rv-RFP (tagged with plasmid pML2570) and H37Rv-ΔRD1-E2-Crimson (tagged with plasmid pTEC19, which was a gift from Lalita Ramakrishnan (Addgene plasmid # 30178) (37). The strains had been routinely tested for PDIM expression as shown in **Supplemental Figure 3**. The protocol is described in the Supplemental materials. The clinical isolates *M. tuberculosis* N0072-EGFP (Lineage 1), *M. tuberculosis* N0145-EGFP (Lineage 2), *M. tuberculosis* N0024-EGFP (Lineage 3) were obtained from Sebastien Gagneux (Basel, Switzerland). Mycobacteria were cultured in Middlebrook's 7H9 broth medium (Sigma-Aldrich, #M0178) supplemented with 10% (v/v) Middlebrook OADC (BD Biosciences, #212351) and 0.05% (v/v) Tween80 (Sigma-Aldrich, #P1754) in 50 ml Falcon tubes at 37°C with rotation. Alternatively, mycobacteria were plated on petri dishes containing Middlebrook's 7H11 agar medium (Sigma-Aldrich, #M0428) supplemented with 10% OADC and incubated at 37°C for 2-3 weeks until colonies appeared.

Infection of hLEC with *M. tuberculosis*

A detailed infection protocol can be found in (19). Briefly, *M. tuberculosis* cultures were grown to mid-exponential phase, washed twice with PBS, once with ECM medium, and then shaken with glass beads to break up bacterial clumps. *M. tuberculosis* were then resuspended in ECM medium and centrifuged at a slow speed to pellet any remaining clumps, but leaving individual bacteria in suspension. The OD_{600} of the bacterial suspension was measured and then added to hLECs at a theoretical multiplicity of infection (MOI) of 10 in ECM medium. Infection was for five hours and was followed by two PBS washes to remove any uninfected *M. tuberculosis*. The infected cells were incubated usually for 2-72 h but up to 7 days for live

cell imaging. For experiments requiring co-infection of two *M. tuberculosis* strains, we used strains tagged with different colours to distinguish between them (RFP, EGFP or E2-Crimson). These strains were prepared individually using the above method, and only mixed just prior to hLEC infection (at an MOI of 5 each, to achieve a total MOI of 10).

For the activation of hLECs with IFNG post-infection, hLECs were infected with *M. tuberculosis* at an MOI of 5 for 72 hours, as described below. After 72hours, human IFNG (Peprotech, #300-02) was added in appropriate wells at a final concentration of 200 ng/mL. Cells were then incubated for an additional 24 hours before being fixed with PBS-PFA 4% solution and processed for immunofluorescence.

Indirect immunofluorescence

An extended method can be found in (19). In summary, infected hLEC on coverslips were fixed with 3% methanol-free paraformaldehyde (Electron Microscopy Sciences, #15710) in PBS for 24 h. Coverslips were quenched with 50 mM NH_4Cl (Sigma-Aldrich, #A9434) and then permeabilised with 0.01% saponin (Sigma-Aldrich, #84510) 1% BSA (Sigma-Aldrich, #A3912) in PBS. The cells were washed with PBS and then 30-50 µl of the primary antibody (diluted in PBS with 0.01% saponin, 1% BSA) was added onto the coverslips for one to two hours at room temperature (detailed in **Supplemental Table 1**). Following this, three PBS washes preceded addition of the secondary antibody (diluted in the same way as the primary antibody) for one hour at room temperature. The coverslips were again washed three times in PBS, before an optional staining step for F-actin using a 1:250 dilution of either rhodamine phalloidin (Biotium, #00027), Alexa Fluor 633-phalloidin (Life Technologies, #A22284) or Alexa Fluor 488-phalloidin (Life Technologies, #A12379) for 20 minutes at room temperature. After three more PBS washes, 300 nM DAPI (Life Technologies, #D3571) in PBS was added for 10 minutes to stain nuclei. After a final PBS wash, the coverslips were mounted onto glass slides using DAKO mounting medium (DAKO Cytomation, #S3023).

Confocal microscope image acquisition and analysis

Imaging of fixed samples was performed using a Leica SP5 AOBS Laser Scanning Confocal Microscope (Leica Microsystems) exactly as detailed in (19). Images were obtained in .lif format and imported into FIJI (NIH). Three parameters were measured using FIJI: a) *M. tuberculosis* growth using the total GFP signal per hLEC; b) The association of a marker (e.g.

Galectin 8) to *M. tuberculosis*; c) Intracellular cord size using Feret diameter. a) and b) are extensively described in (19), whereas Feret diameter is explained in **Supplemental Figure 1**. All data were plotted and analysed using Microsoft Excel 2010 (Microsoft), GraphPad Prism 6 (GraphPad Software Inc.) or ggplot2 (Hadley Wickham) in R (The R Project for Statistical Computing).

Automated confocal microscope image acquisition and analysis

After infection in a 96 wells plate, cells were fixed and stained with DAPI, and fluorescently-labelled phalloidin (conjugated with Alexa Fluor 633 or Alexa Fluor 488). Images were acquired using an automated fluorescent confocal microscope (OPERA Phenix, PerkinElmer) equipped with a 63X (NA 1.2) water lens and 405, 488, 561 and 640 nm excitation lasers. The emitted fluorescence was captured using 2 cameras associated with a set of filters covering a detection wavelength ranging from 450 to 690 nm. For each well, 30 to 35 adjoining fields containing 4 Z-stacks distant from 1µm were acquired. 10% overlap was applied between fields in order to generate a global image clustering all the fields in a single image. The maximum projection of the images was analysed using a dedicated in-built script developed using the image-analysis software Harmony 4.6 (PerkinElmer).

Cell segmentation: A local intensity detection algorithm applied on the DAPI channel was used to detect both Nuclei and cytoplasm (nuclei: maximal local intensity; cytoplasm: minimal local intensity).

Intracellular bacteria detection: A spot detection algorithm based on the GFP, RFP or Far Red channel (according to the fluorophore expressed by the bacterial strains) was applied for the detection of intracellular fluorescent-M. tuberculosis H37Rv (WT), H37Rv-ΔPDIM or H37Rv-ΔRD1. A manual threshold method, using non-infected wells, was applied to determine the background threshold. These spots were defined as region of interest (ROI) for the measurement of bacterial intensity and area in pixels. The relative bacterial load was expressed in bacterial area (pixel) per cell. The intracellular bacterial growth was quantified by the ratio of intracellular bacterial area per cell between T0 (5h.pi=uptake) and 3 days post-infection. For the quantification of the Feret diameter, the global image of the bacteria channel was exported from Harmony in .png before being converted in 8bit image and analysed in Fiji as previously described [(19) and **Supplemental Figure 1**].

Live cell imaging

hLEC were seeded and infected as previously described. 24 hours prior to infection, the cells were transduced with LentiBrite RFP-p62 Lentiviral Biosensor (Merck Millipore, #17-10404) using an MOI of 40 according to the manufacturer's instructions. After infection of hLEC, the live cell dishes were placed in a holder custom-made for confocal microscopy in a Biosafety Level 3 (BSL-3) laboratory and imaged using the following conditions: 15 min frame intervals, Z-stacks of 5 slices with 1.38 µm thickness, line averaging 4 and zoom of 1.

Electron microscopy (EM) of single-infected cells

Electron microscopy was performed exactly as previously described (19). Briefly, hLEC were infected for 5 + 72 hours with *M. tuberculosis* WT-EGFP prior to fixation in 4% PFA/2.5% GA in 0.1 M phosphate buffer for 24 hours at 4°C. The field of view of interest was imaged first by confocal microscopy, and then processed for imaging by serial block face scanning electron microscopy (SBF SEM) using a 3View2XP (Gatan, Pleasanton, CA) attached to a Sigma VP SEM (Zeiss, Germany). The same field of view was captured thus facilitating the creation of a composite correlative light/electron microscopy (CLEM) image. SBF SEM images were collected at 1.8 kV using the high current setting with a 20 µm aperture at 5-10 Pa chamber pressure and a 2 µs dwell time. Maximum intensity projections of confocal slices were aligned manually to highlight bacteria positions.

Measurement of intracellular *M. tuberculosis* volumes

Selected bacteria were segmented manually from slices of SBF SEM datasets and 3D reconstructions were made using the 3dmod program of IMOD (Kremer et al., 1996). Each dataset was first de-noised with a 0.5 pixel Gaussian blur filter applied in Fiji (ImageJ; National Institutes of Health). 2 datasets from each of 2 independent samples were then segmented for each of the cord and membrane-bound bacteria conditions. The dataset xy pixels were 9.9 nm and 8.7 nm for cord bacteria, and 5.4 nm and 6.3 nm for membrane bound bacteria; all datasets consisted of serial images of 50 nm thickness. The dataset dimensions were 81.1 x 81.1 x 5.55, 71.3 x 71.36 x 1, 22.1 x 22.1 x 1.55, 51.6 x 51.6 x 2.75 µm in xyz, with 111, 20, 31, and 55 serial images, respectively. To calculate bacterial volumes, IMOD calculated Volume Inside Mesh using 3D mesh structures derived from closed contours drawn around bacteria each 50 nm, using imodmesh. For CLEM of representative 3D reconstructions of bacteria, an

SBF SEM slice was assigned to a confocal slice manually in z. The confocal slice was then processed in Fiji; first, to improve interpolation during TurboReg alignment, the confocal image was upscaled from 1024 to 2048 pixels with a bilinear interpolation, and a Smooth filter applied twice; then TurboReg was then used to align the processed confocal slice with the SBF SEM image using a Scaled Rotation transformation and bacteria as landmarks (identified by fluorescence and morphology). The remaining SBF SEM images in the stack were further denoised with a 1 pixel Gaussian blur filter and brightness/contrast adjusted to match the CLEM image in Photoshop. The CLEM image was then inserted into the stack, and a Snapshot taken of the bacterial segmentation with the stack in the Model view of 3dmod.

CLEM of co-infected cells

hLEC were co-infected with *M. tuberculosis* WT-RFP and M. tuberculosis ΔRD1-GFP prior to fixation and confocal microscopy as above. The field of interest was then processed for imaging by transmission electron microscopy (TEM). The cells were post-fixed in 1% reduced osmium tetroxide, stained with tannic acid, and quenched in 1% sodium sulphate. Next, the cells were dehydrated progressively up to 100% ethanol and incubated in a 1:1 propylene oxide/epon resin mixture. After infiltrations in pure resin, the samples were embedded at 60°C for 24 h. SBF SEM and TEM was performed as described previously (38). Briefly, the field of interest was approached by SBF SEM (there being sufficient signal for approach imaging even though the cells were not processed for this method), then the cut face was aligned to a diamond knife in a UC7 ultramicrotome (Leica Microsystems) and 70-80 nm sections from the field of interest were collected. The sections were stained with lead citrate and imaged in a TEM (Tecnai G2 Spirit BioTwin; Thermo Fisher Scientific) using a charge-coupled device camera (Orius; Gatan Inc.). For CLEM overlay, TEM images were assigned to confocal slices manually in z. The confocal slice was then processed and aligned with TurboReg in Fiji as above.

Histology, immunohistochemistry and analysis

Formalin-fixed paraffin-embedded cervical lymph nod tissue sections from patients diagnosed as tuberculosis culture positive and/or acid-fast bacilli positive (AFB+) were selected for the study and processed as described before (19). Briefly, tissue sections were deparaffinized in xylene (2 x 10 min, 100%, 95% and 80% ethanol (2 min each). Tissue sections

were then placed into an antigen retrieval buffer (Access super antigen solution, Menarini diagnostics, UK) in a decloaking chamber (Biocare Medical, CA, USA); incubated at 110 degrees for 10 min and allowed to cool for 60 min. Sections were permeabilized in PBS-0.2% Triton X-100 and incubated in blocking buffer (1% BSA, 5% Fetal Calf Serum in PBS) overnight at room temperature. Tissue sections were labelled using primary antibodies rabbit anti-Mtb (Menapath, 1:100 dilution) and rat anti-PDPN (BioLegend, USA, #337002, 1:200 dilution). Secondary antibodies used were a goat anti-rabbit Alexa Fluor 488 and a goat anti-rat Alexa Fluor 568 (Lifetechnologies, #A11077 and #A11034, respectively, dilution 1/800). Primary and secondary antibodies were tested for cross reaction in samples of uninfected individuals. Primary (human antigens) and secondary antibodies for cross-reaction with *M. tuberculosis* in samples that were acid fast positive (AFB+).

RNA extraction and sequencing library preparation

M. tuberculosis-infected or uninfected hLECs (48 hours infection) were lysed in 0.5mL of TRIzol and RNA was extracted using Direct-zol RNA MiniPrep Kit (Zymo Research) and treated with TURBO DNase I (Life Technologies) until DNA-free. Quantity and quality of the extracted RNA were determined by Qubit flourometer, NanoDrop spectrophotometer and Bioanalzyer. RNA-Seq libraries were prepared using 1mg of RNA of each sample with TruSeq Stranded Total RNA Library Prep kit (Illumina) and ribosomal RNA was removed with Ribo-Zero as part of the library construction process. Quality and quantity of the cDNA libraries were determined by Qubit flourometer and Bioanalzyer before being processed for sequencing with Illumina Hi-Seq 2500 for single-end reads with 100 cycles.

RNA-Seq data analysis

The RNA-Seq data in this paper have been deposited in Gene Expression Omnibus repository with accession number **GSE110564**. The quality of the Illumina-produced fastq files was assessed using FastQC (v0.11.5) and adapter trimmed using Trimmomatic (v0.36). The resulting reads were then aligned to the human genome (Ensembl GRCh38 release 88 build) using STAR aligner (v2.5.2a). Gene counting was done using RSEM (v1.2.29) and expected read counts were normalized using DESeq2 (v1.18.1), which also determined the log2 fold change and statistical significance between the infected and uninfected samples. Canonical pathway and functional process analyses were performed using IPA Ingenuity (QIAGEN) and MetaCore

(Thomson Reuters). The expression of several genes had been confirmed by RT-qPCR as described in Supplemental materials.

Data and statistical analysis

Results are expressed as mean ± SEM. All statistical analyses were performed in Prism 6 (GraphPad Software Inc.). Means between 2 groups were compared using two-tailed Student's *t* tests and means among 3 or more groups were compared using one-way ANOVA with Tukey's multiple comparisons tests. A *p* value of under 0.05 was considered significant (*p<0.05; ** p<0.01, *** p<0.001, ns: no significant). Plots were produced in Prism 6 or ggplot2 in R (The R Project for Statistical Computing).

Study approval

The study was performed using excised cervical lymph node tissue stored within the Department of Anatomical Pathology at Groote Schuur Hospital (Cape Town, South Africa). All of these biopsies were taken for clinical indications. Residual paraffin-embedded blocks of these specimens were stored for further processing. This study complied with the Declaration of Helsinki (2008), and ethics approval was obtained from the University of Cape Town Human Research Ethics Committee (REC187/2013). Informed consent was waived, as this was a retrospective study of formalin-fixed paraffin-embedded tissue samples collected during the course of routine clinical practice. Patient identifiers were unavailable to investigators.

Author contributions

MGG and TRL conceived the project. MGG, TRL, CJQ and RPL designed the experiments. TRL, CJQ, RPL, MGR, AF and CQJ performed experiments. TRL, CJQ, RPL, MGR, AF, LC, DJG and RJW analysed data and provided intellectual input. MGG wrote the manuscript with input from TRL and CJQ. All authors read the manuscript and provided critical feedback.

Acknowledgements

We thank J. Kendrick-Jones (MRC-LMB, Cambridge) for NDP52 antibody and Michael Niederweis (University of Alabama) for fluorescent plasmids. Bill Jacobs (Albert Einstein College of Medicine), Suzie Hingley-Wilson (University of Surrey), Catherine Astaire-Dequeuer (IPBS, Toulouse), Douglas Young (Francis Crick, Institute, London) and Sebastien Gagneux

(THP, Basel) for *M. tuberculosis* strains, Steve Coade for assistance with fluorescent tagging of clinical isolates and Susanne Herbst for critical reading of the manuscript. This work was supported by the Francis Crick Institute (to MGG and RJW), which receives its core funding from Cancer Research UK (FC001092, FC00110218), the UK Medical Research Council (FC001092, FC00110218), and the Wellcome Trust (FC001092, FC00110218) and Wellcome Trust (to RJW, 104803, 203135).

References:

1. (WHO) WHO. Global TB report. 2019.
2. Koch R. Die Äetiologie der Tuberkulose. *Berliner klinische Wochenschrift.* 1882;15: 221–230.
3. Glickman MS, Cox JS, and Jacobs WR, Jr. A novel mycolic acid cyclopropane synthetase is required for cording, persistence, and virulence of Mycobacterium tuberculosis. *Mol Cell.* 2000;5(4):717-27.
4. Middlebrook G, Dubos RJ, and Pierce C. Virulence and Morphological Characteristics of Mammalian Tubercle Bacilli. *J Exp Med.* 1947;86(2):175-84.
5. Hunter RL, Olsen MR, Jagannath C, and Actor JK. Multiple roles of cord factor in the pathogenesis of primary, secondary, and cavitary tuberculosis, including a revised description of the pathology of secondary disease. *Ann Clin Lab Sci.* 2006;36(4):371-86.
6. Hunter RL, Venkataprasad N, and Olsen MR. The role of trehalose dimycolate (cord factor) on morphology of virulent M. tuberculosis in vitro. *Tuberculosis (Edinb).* 2006;86(5):349-56.
7. Indrigo J, Hunter RL, Jr., and Actor JK. Influence of trehalose 6,6'-dimycolate (TDM) during mycobacterial infection of bone marrow macrophages. *Microbiology.* 2002;148(Pt 7):1991-8.
8. Bernut A, Herrmann JL, Kissa K, Dubremetz JF, Gaillard JL, Lutfalla G, et al. Mycobacterium abscessus cording prevents phagocytosis and promotes abscess formation. *Proc Natl Acad Sci U S A.* 2014;111(10):E943-52.
9. Maximow A. *Annis Inst Pasteur.* 1928;42:225.
10. Shepard CC. Growth characteristics of tubercle bacilli and certain other mycobacteria in HeLa cells. *J Exp Med.* 1957;105(1):39-48.
11. Ferrer NL, Gomez AB, Soto CY, Neyrolles O, Gicquel B, Garcia-Del Portillo F, et al. Intracellular replication of attenuated Mycobacterium tuberculosis phoP mutant in the absence of host cell cytotoxicity. *Microbes Infect.* 2009;11(1):115-22.
12. Kalsum S, Braian C, Koeken V, Raffetseder J, Lindroth M, van Crevel R, et al. The Cording Phenotype of Mycobacterium tuberculosis Induces the Formation of Extracellular Traps in Human Macrophages. *Front Cell Infect Microbiol.* 2017;7:278.
13. Wong KW, and Jacobs WR, Jr. Mycobacterium tuberculosis exploits human interferon gamma to stimulate macrophage extracellular trap formation and necrosis. *J Infect Dis.* 2013;208(1):109-19.
14. Galluzzi L, Baehrecke EH, Ballabio A, Boya P, Bravo-San Pedro JM, Cecconi F, et al. Molecular definitions of autophagy and related processes. *EMBO J.* 2017;36(13):1811-36.
15. Deretic V, and Levine B. Autophagy, immunity, and microbial adaptations. *Cell Host Microbe.* 2009;5(6):527-49.
16. Gutierrez MG, Master SS, Singh SB, Taylor GA, Colombo MI, and Deretic V. Autophagy is a defense mechanism inhibiting BCG and Mycobacterium tuberculosis survival in infected macrophages. *Cell.* 2004;119(6):753-66.
17. Watson RO, Manzanillo PS, and Cox JS. Extracellular M. tuberculosis DNA targets bacteria for autophagy by activating the host DNA-sensing pathway. *Cell.* 2012;150(4):803-15.

18. Deretic V, Delgado M, Vergne I, Master S, De Haro S, Ponpuak M, et al. Autophagy in immunity against mycobacterium tuberculosis: a model system to dissect immunological roles of autophagy. *Curr Top Microbiol Immunol.* 2009;335:169-88.
19. Lerner TR, de Souza Carvalho-Wodarz C, Repnik U, Russell MR, Borel S, Diedrich CR, et al. Lymphatic endothelial cells are a replicative niche for Mycobacterium tuberculosis. *The Journal of clinical investigation.* 2016;126(3):1093-108.
20. Romagnoli A, Etna MP, Giacomini E, Pardini M, Remoli ME, Corazzari M, et al. ESX-1 dependent impairment of autophagic flux by Mycobacterium tuberculosis in human dendritic cells. *Autophagy.* 2012;8(9):1357-70.
21. Kimmey JM, Huynh JP, Weiss LA, Park S, Kambal A, Debnath J, et al. Unique role for ATG5 in neutrophil-mediated immunopathology during M. tuberculosis infection. *Nature.* 2015;528(7583):565-9.
22. Behr MA, and Waters WR. Is tuberculosis a lymphatic disease with a pulmonary portal? *Lancet Infect Dis.* 2014;14(3):250-5.
23. Ganchua SKC, Cadena AM, Maiello P, Gideon HP, Myers AJ, Junecko BF, et al. Lymph nodes are sites of prolonged bacterial persistence during Mycobacterium tuberculosis infection in macaques. *PLoS pathogens.* 2018;14(11):e1007337.
24. Patterson KC, Queval CJ, and Gutierrez MG. Granulomatous Inflammation in Tuberculosis and Sarcoidosis: Does the Lymphatic System Contribute to Disease? *Bioessays.* 2019;41(11):e1900086.
25. Ganbat D, Seehase S, Richter E, Vollmer E, Reiling N, Fellenberg K, et al. Mycobacteria infect different cell types in the human lung and cause species dependent cellular changes in infected cells. *BMC Pulm Med.* 2016;16:19.
26. Lerner TR, Borel S, and Gutierrez MG. The innate immune response in human tuberculosis. *Cellular microbiology.* 2015;17(9):1277-85.
27. Randall PJ, Hsu NJ, Quesniaux V, Ryffel B, and Jacobs M. Mycobacterium tuberculosis infection of the 'non-classical immune cell'. *Immunol Cell Biol.* 2015;93(9):789-95.
28. Nair VR, Franco LH, Zacharia VM, Khan HS, Stamm CE, You W, et al. Microfold Cells Actively Translocate Mycobacterium tuberculosis to Initiate Infection. *Cell Rep.* 2016;16(5):1253-8.
29. Lerner TR, Borel S, Greenwood DJ, Repnik U, Russell MR, Herbst S, et al. Mycobacterium tuberculosis replicates within necrotic human macrophages. *J Cell Biol.* 2017;216(3):583-94.
30. Lerner TR, Queval CJ, Fearns A, Repnik U, Griffiths G, and Gutierrez MG. Phthiocerol dimycocerosates promote access to the cytosol and intracellular burden of Mycobacterium tuberculosis in lymphatic endothelial cells. *BMC Biol.* 2018;16(1):1.
31. Astarie-Dequeker C, Le Guyader L, Malaga W, Seaphanh FK, Chalut C, Lopez A, et al. Phthiocerol dimycocerosates of M. tuberculosis participate in macrophage invasion by inducing changes in the organization of plasma membrane lipids. *PLoS pathogens.* 2009;5(2):e1000289.
32. Augenstreich J, Arbues A, Simeone R, Haanappel E, Wegener A, Sayes F, et al. ESX-1 and phthiocerol dimycocerosates of Mycobacterium tuberculosis act in concert to cause phagosomal rupture and host cell apoptosis. *Cellular microbiology.* 2017;19(7).
33. Quigley J, Hughitt VK, Velikovsky CA, Mariuzza RA, El-Sayed NM, and Briken V. The Cell Wall Lipid PDIM Contributes to Phagosomal Escape and Host Cell Exit of Mycobacterium tuberculosis. *mBio.* 2017;8(2).
34. Hunter RL, Hwang SA, Jagannath C, and Actor JK. Cord factor as an invisibility cloak? A hypothesis for asymptomatic TB persistence. *Tuberculosis (Edinb).* 2016;101S:S2-S8.
35. Kaplan G, Post FA, Moreira AL, Wainwright H, Kreiswirth BN, Tanverdi M, et al. Mycobacterium tuberculosis growth at the cavity surface: a microenvironment with failed immunity. *Infect Immun.* 2003;71(12):7099-108.

36. Rao V, Fujiwara N, Porcelli SA, and Glickman MS. Mycobacterium tuberculosis controls host innate immune activation through cyclopropane modification of a glycolipid effector molecule. *J Exp Med.* 2005;201(4):535-43.
37. Takaki K, Davis JM, Winglee K, and Ramakrishnan L. Evaluation of the pathogenesis and treatment of Mycobacterium marinum infection in zebrafish. *Nat Protoc.* 2013;8(6):1114-24.
38. Russell MR, Lerner TR, Burden JJ, Nkwe DO, Pelchen-Matthews A, Domart MC, et al. 3D correlative light and electron microscopy of cultured cells using serial blockface scanning electron microscopy. *J Cell Sci.* 2017;130(1):278-91.

Figure Legends

Figure 1: *M. tuberculosis* forms extensive intracellular cords in hLECs and lymph node biopsies

(A) Images of primary human lymphatic endothelial cells (hLEC) infected with GFP expressing *M. tuberculosis* for 2-72 h. Over time, *M. tuberculosis* grows and forms large intracellular cords. Nuclei are stained with DAPI (blue) and F-actin is stained by rhodamine phalloidin (red). **(B)** 3D reconstruction of Z-stacks taken of an intracellular cord from (A). Various angles are shown to confirm that the cord is completely encapsulated within the host cell. **(C)** Measurement of the intracellular cords over time in hLEC using the Feret diameter (see **Supplemental Figure 1**) showing that the cords elongate over time up to a maximum of 150 µm. The number of bacterial clusters analysed are: 418 (2h), 233 (24h), 814 (48h), 618 (72h) and were obtained from three independent experiments. One-way ANOVA with Tukey's multiple comparisons tests: *** = $p < 0.001$ **(D)** Image of A549 cells infected with *M. tuberculosis*-EGFP for 72 h showing an intracellular cord looping around the nucleus. Nuclei are stained with DAPI (blue) and F-actin is stained with rhodamine phalloidin (red). **(E)** Intracellular cord formation after 72 h was also observed in hLEC infected with representative strains from three other *M. tuberculosis* lineages: N0072 (lineage 1), N0145 (lineage 2), N0024 (lineage 3). Images displayed in **D** and **E** are representative of at least three independent experiments **(F)** Tissue section of a granuloma present in a human lymph stained for acid fast bacilli (AFB). Zoomed region shows association of *M. tuberculosis* cords with cells (black boxes). Representative histological sections from human patients after lymph node tissue resection surgery were stained for podoplanin (PDPN), *M. tuberculosis* and nuclei (DAPI).

735 Scale bar is 1 mm. White boxes delimit the zoomed regions displayed on the right-hand side.
736 Arrows indicate the presence of *M. tuberculosis* cords within PDPN+ cells. Scale bar is 20 µm.
737
738 **Figure 2: *M. tuberculosis* induces cytosolic surveillance and host pro-survival pathways**
739 **(A)** Top 10 functional process analysis hits by false-discovery rate (FDR) of genes significantly
740 upregulated in hLECs 48 h post-infection, indicated by RNAseq. '% in Data' indicates the % of
741 genes in the annotation group that were significantly upregulated in the analysis. **(B)** Heatmap
742 of significantly upregulated (padj < 0.05) genes 48 h post infection grouped by sensing
743 pathway reveal an induction of pro-inflammatory, DNA, RNA and glycan sensing pathways
744 and **(C)** genes involved in antigen presentation and the negative regulation of cell death.
745 Significance of RNA-seq data add been calculated from 3 independent experiments (**D**) qPCR
746 confirmation of key infection-response pathways 48 h post infection. Data are representative
747 of three independent experiments, each performed in triplicate. Student's *t* tests: ** =
748 p<0.01; *** = p<0.001; ns: no significant.
749
750 **Figure 3: Intracellular cords are localised in the host cell cytosol and consist of chains of *M.***
751 ***tuberculosis* of a small size.**
752 **(A-B)** Correlative light electron microscopy (CLEM) images of hLEC infected with *M.*
753 *tuberculosis*-GFP. Top left subpanel shows the light microscopy images, with the
754 corresponding electron microscopy images in the top right subpanel. The larger subpanels
755 show a composite of the fluorescence overlaid onto the electron microscopy. **(A)** *M.*
756 *tuberculosis* intracellular cord, without any encapsulating host membrane, indicating that it
757 is present in the cytosol. **(B)** *M. tuberculosis* encapsulated in a membranous compartment, as
758 a control for confirming membrane preservation due to the sample preparation. Host cell
759 membrane is highlighted in red. **(C-D)** To quantify the volume of *M. tuberculosis*, individual
760 bacteria were manually segmented from slices of SBF SEM images and 3D reconstructions of
761 selected bacteria were made (coloured rods), using 3dmod. Representative reconstructions
762 are shown, with corresponding fluorescence highlighted (matched manually with the
763 corresponding SBF SEM slice in Z, and then aligned in xy with TurboReg in Fiji). Dataset
764 dimensions; (**C**) Left panel: 8.7 x 8.7 x 50 nm pixels, Right panel: 71.3 x 71.36 x 1 µm in xyz; (**D**)
765 Left panel: 6.3 x 6.3 x 50 nm pixels; Right panel: 51.6 x 51.6 x 2.75 µm in xyz. **(E)** The volume
766 of each bacterium reconstruction from two independent sample datasets was calculated in

3dmod, and a comparison between those in a membrane bound compartment and those in an intracellular cord was made. The data ± SEM show that individual bacteria forming cords are significantly smaller. Student's t-test: ** = p <0.01.

Figure 4: *M. tuberculosis* lacking RD1 locus or PDIMs expression fail to cord within hLECs

(A) hLEC were infected with RFP-expressing *M. tuberculosis* WT, GFP-expressing *M. tuberculosis* ΔPDIM or E2-Crimson-expressing ΔRD1 for 72 h at a MOI of 10, fixed and stained for F-actin with AF633 or AF488-phalloidin. Either deleting PDIM or the RD1 locus abolished cord formation. WT bacteria (red), ΔPDIM and ΔRD1-bacteria (green), F-actin (white) and nuclei (blue). Scale bar is 50 µm. **(B)** Feret diameter measurements from three independent experiments were plotted. For each condition tested, the number of bacterial clusters analysed is between 600 and 1,200 **(C)** hLEC were infected for 72 h with RFP-expressing *M. tuberculosis* WT at a MOI of 10, or with E2-Crimson-expressing *M. tuberculosis* ΔRD1 at a MOI of 10, 20 or 40. WT bacteria (red), ΔRD1-bacteria (green), F-actin (white) and nuclei (blue). Scale bar is 50 µm. **(D)** Feret diameter measurements from images in (C) from two independent experiments were plotted. The number of bacterial clusters analysed are: 3,960 for WT and 6,470, 9,472, 11,759 for ΔRD1 at MOI:10, 20 and 40, respectively. (**E**) Quantification of the bacterial load per cell, expressed in bacterial area (μm^2) per cell, following the uptake (5h.pi) and 72h post infection. (**F**) Intracellular bacterial growth after 72h infection, expressed by the ratio bacterial area per cell 72h.pi/5h.pi. Values > 1 represent the bacterial growth. (**E** and **F**) Data ± SEM are representative of two independent experiments performed in duplicate. (**B**, **C**, **D** and **E**) One-way ANOVA with Tukey's multiple comparisons tests against WT: ** = p<0.01; *** = p <0.001; ns: no significant.

Figure 5: Access to the cytosol is required for *M. tuberculosis* intracellular cording

(A) hLEC were infected for 72 h with *M. tuberculosis* WT-RFP (red), *M. tuberculosis*-ΔPDIM-GFP (green), *M. tuberculosis*-ΔRD1-E2-Crimson (green) either individually or as a co-infection WT-RFP/ΔPDIM-GFP or WT-RFP/ΔRD1-E2-Crimson. Cells were then fixed and stained for F-actin with AF633 or AF488-phalloidin (Both visualized in white) and DAPI (blue). Scale bar is 10 µm. The images show that during single infection, *M. tuberculosis* WT exhibits intracellular cording, whereas *M. tuberculosis* ΔPDIM or ΔRD1 do not. However, in the co-infected sample, both *M. tuberculosis* ΔPDIM and ΔRD1 were able to form intracellular cords. **(B)** Feret

diameter measurements from images in **(A)** were plotted. n represent the number of bacterial clusters analysed. **(C)** Intracellular bacterial growth after 72h infection, expressed by the ratio bacterial area per cell 72h.pi/5h.pi. Values > 1 represent the bacterial growth. **(A-C)** Data ± SEM are representative of three independent experiments. One-way ANOVA with Tukey's multiple comparisons tests: * = p<0.05; ** = p<0.01; *** = p <0.001.

(D-E) Co-infected hLEC samples were processed for correlative light electron microscopy (CLEM) to confirm at the ultrastructural level that *M. tuberculosis* ΔRD1-GFP cords were indeed present in the cytosol (E; magnifications of regions indicated in D, asterisks mark cytosolic bacteria).

Figure 6: Intracellular cords are not recognized by cytosolic immune sensors in both resting or IFN-γ-activated hLECs.

(A-C) Live cell imaging of hLEC expressing p62-RFP (red) infected with *M. tuberculosis*-GFP (green) for 115 h. Imaging started 15 min after addition of the bacteria to the cells. Snapshots from the movies (**Supplemental Movies 1-3**) are shown, with the timepoint displayed above in hh:mm:ss format. Scale bars are 10 µm. **(A)** The pink arrow tracks an example of an intracellular cord forming from a single bacterium, which never interacts/associates with p62. **(B)** The blue arrow tracks an example of an individual *M. tuberculosis* bacterium becoming associated to p62 throughout which leads to restriction of growth. **(C)** The blue arrow tracks an example of *M. tuberculosis* associating and dissociating with p62 multiple times. Only after p62 association ceased completely, cord formation started. **(c-e, right hand panel)** ImageJ quantification of the GFP intensity and the p62-RFP association of the arrowed bacteria over time. Letters a-f refer to the snapshots in **(A-C)**. **(D)** Representative image of hLEC infected *M. tuberculosis* WT-EGFP (blue) for 72 h and stained for the autophagy adaptor p62 (red) and the autophagy receptor ubiquitin (Ub) (green). Cell nuclei are stained with DAPI (blue). Scale bar is 10 µm. **(E)** Intracellular markers of autophagy, pathogen sensing were assessed for their association to intracellular cords 72 h post infection. Particles with a Feret diameter greater than 10 µM were considered cords, and a marker association score above 100 was considered positive. Points correspond to individual bacterial particles. **(F and G)** Representative image of hLEC infected *M. tuberculosis* WT-EGFP (green) for 72 h to let bacteria forming intracellular cords before being treated or not with 200 ng/mL of human IFNG for an additional 24 hour. Cell were then fixed and stained for the autophagy adaptor p62 (**F**, left panel) or LC3 (**G**, left

831 panel). Both p62 and LC3 markers are visualized in red, cell nuclei are stained with DAPI (blue).
832 Scale bar is 10 µm. Intracellular markers p62 (**F**, right panel) and LC3 (**G**, right panel) were
833 assessed for their association to intracellular bacteria in function of the size of the bacterial
834 cluster. Particles with a Feret diameter greater than 10 µM were considered cords, and a
835 marker association score above 15, 000 for p62 and 10, 000 for LC3 were considered positive.
836 **(D-G)** Data were obtained from three independent experiments, each performed in duplicate.

Figure 1

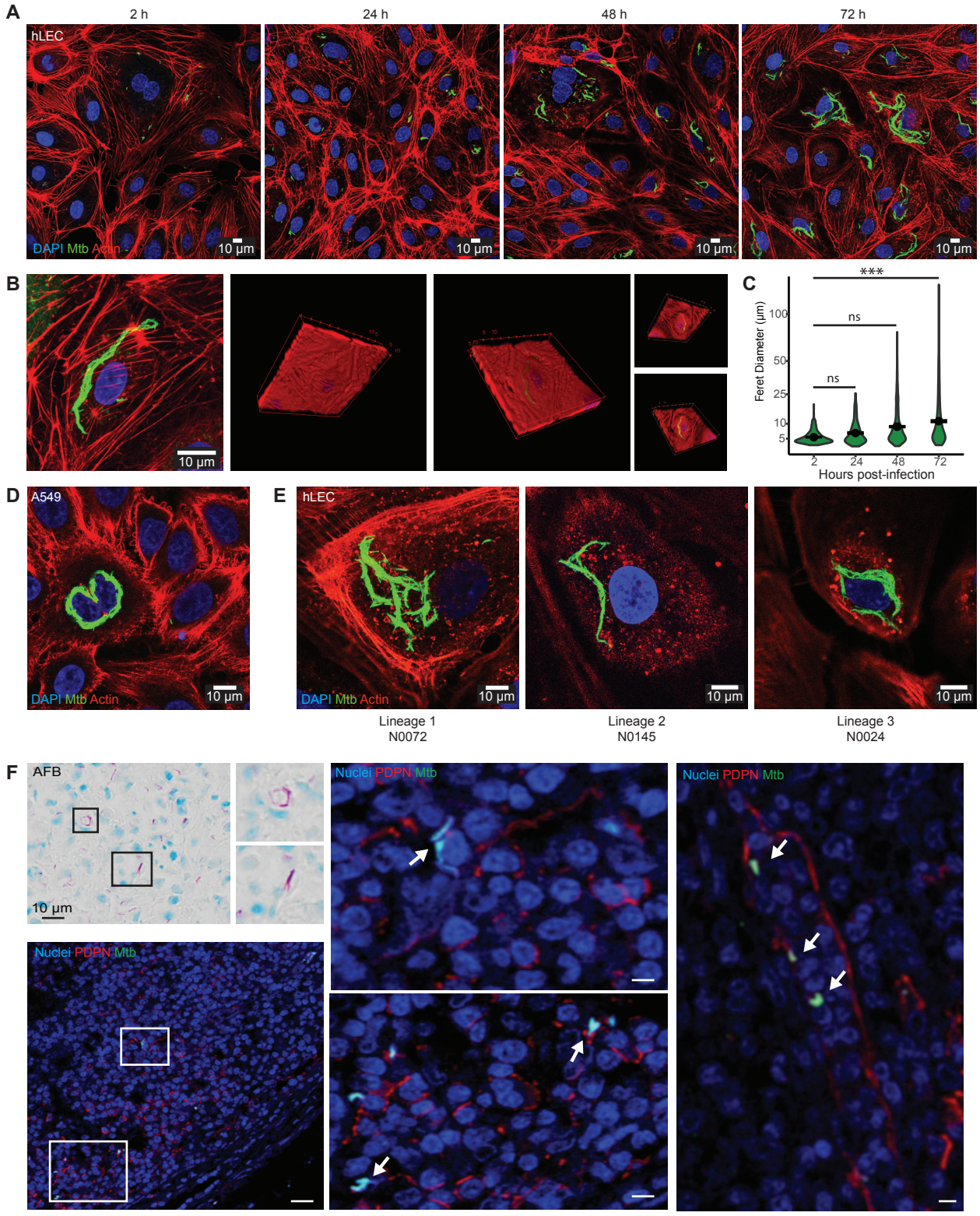

Figure 1: M. tuberculosis forms extensive intracellular cords in hLECs and lymph node biopsies

(A) Images of primary human lymphatic endothelial cells (hLEC) infected with GFP expressing M. tuberculosis for 2-72 h. Over time, M. tuberculosis grows and forms large intracellular cords. Nuclei are stained with DAPI (blue) and F-actin is stained by rhodamine phalloidin (red). (B) 3D reconstruction of Z-stacks taken of an intracellular cord from (A). Various angles are shown to confirm that the cord is completely encapsulated within the host cell. (C) Measurement of the intracellular cords over time in hLEC using the Feret diameter (see Supplemental Figure 1) showing that the cords elongate over time up to a maximum of 150 µm. The number of bacterial clusters analysed are: 418 (2h), 233 (24h), 814 (48h), 618 (72h) and were obtained from three independent experiments. One-way ANOVA with Tukey's multiple comparisons tests: *** = $p < 0.001$ (D) Image of A549 cells infected with M. tuberculosis-EGFP for 72 h showing an intracellular cord looping around the nucleus. Nuclei are stained with DAPI (blue) and F-actin is stained with rhodamine phalloidin (red). (E) Intracellular cord formation after 72 h was also observed in hLEC infected with representative strains from three other M. tuberculosis lineages: N0072 (lineage 1), N0145 (lineage 2), N0024 (lineage 3). Images displayed in D and E are representative of at least three independent experiments (F) Tissue section of a granuloma present in a human lymph stained for acid fast bacilli (AFB). Zoomed region shows association of M. tuberculosis cords with cells (black boxes). Representative histological sections from human patients after lymph node tissue resection surgery were stained for podoplanin (PDPN), M. tuberculosis and nuclei (DAPI). Scale bar is 1 mm. White boxes delimit the zoomed regions displayed on the right-hand side. Arrows indicate the presence of M. tuberculosis cords within PDPN+ cells. Scale bar is 20 µm.

Figure 2

A

Network	% in Data	FDR
Inflammation Interferon signaling	50.0	1.890×10^{-24}
Immune response Antigen presentation	29.4	9.872×10^{-13}
Immune response Innate immune response to RNA viral infection	40.5	9.561×10^{-12}
Immune response Th17-derived cytokines	35.7	2.397×10^{-10}
Inflammation IFN-gamma signaling	32.1	5.936×10^{-09}
Immune response Phagosome in antigen presentation	23.5	1.434×10^{-08}
Inflammation Jak-STAT Pathway	25.3	3.250×10^{-08}
Inflammation MIF signaling	27.9	3.728×10^{-08}
Inflammation IL-10 anti-inflammatory response	33.3	4.600×10^{-08}
Inflammation Innate inflammatory response	25.0	7.400×10^{-08}

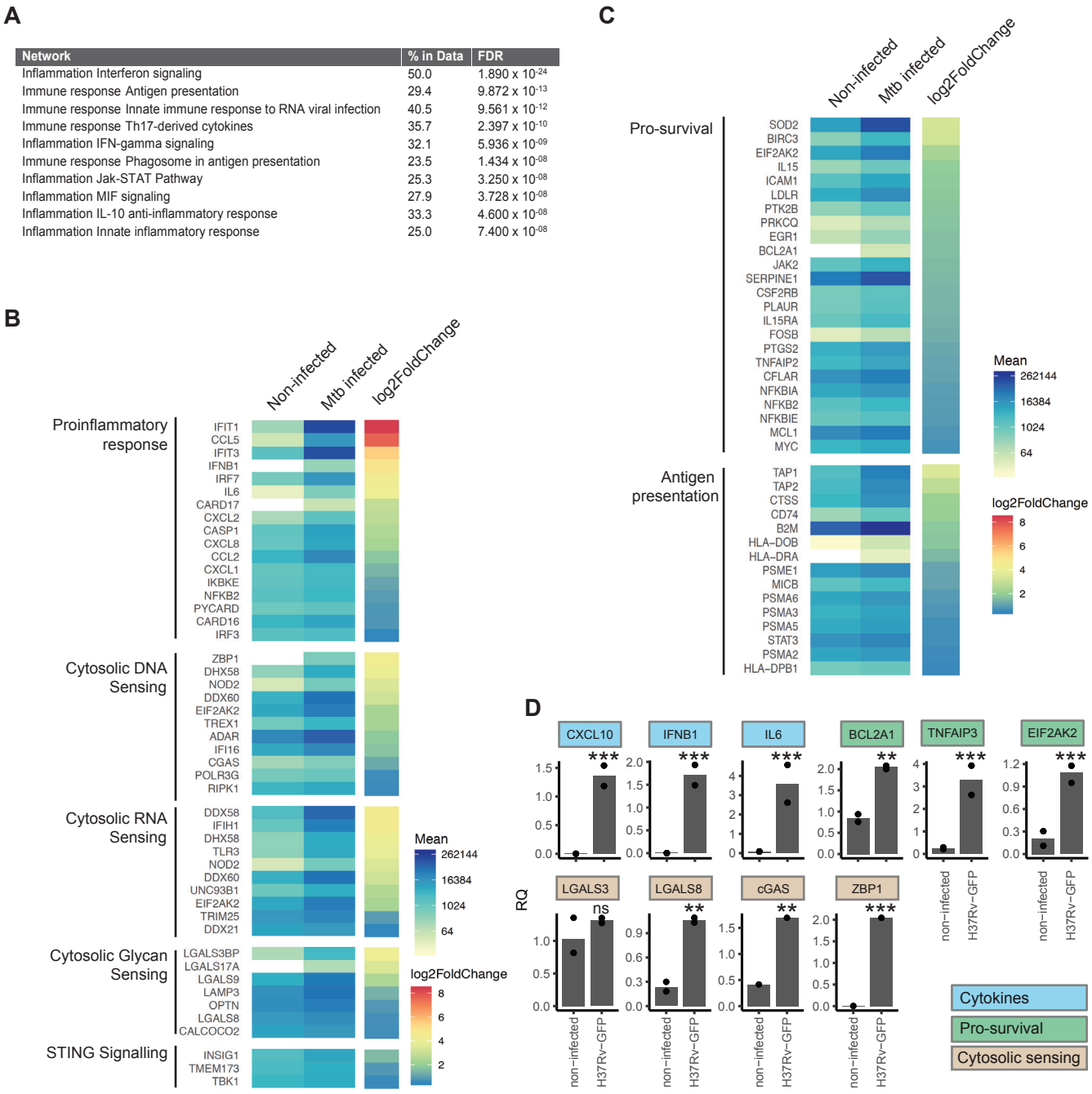

Figure 2: M. tuberculosis induces cytosolic surveillance and host pro-survival pathways
(A) Top 10 functional process analysis hits by false-discovery rate (FDR) of genes significantly upregulated in hLECs 48 h post-infection, indicated by RNAseq. '% in Data' indicates the % of genes in the annotation group that were significantly upregulated in the analysis. (B) Heatmap of significantly upregulated (padj < 0.05) genes 48 h post infection grouped by sensing pathway reveal an induction of pro-inflammatory, DNA, RNA and glycan sensing pathways and (C) genes involved in antigen presentation and the negative regulation of cell death. Significance of RNA-seq data add been calculated from 3 independent experiments (D) qPCR confirmation of key infection-response pathways 48 h post infection. Data are representative of three independent experiments, each performed in triplicate. Student's t tests: ** = p<0.01; *** = p<0.001; ns: no significant.

Figure 3

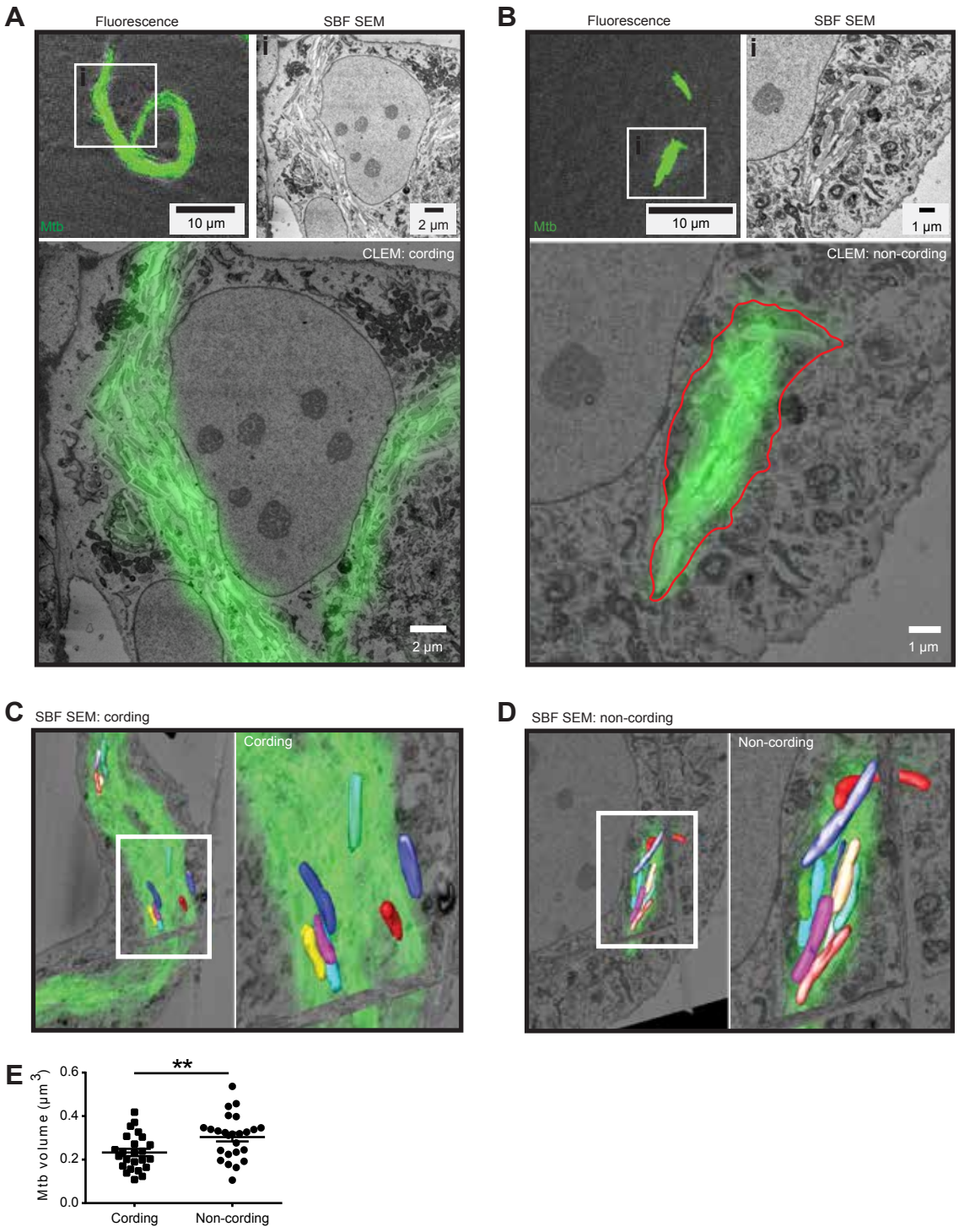

Figure 3: Intracellular cords are localised in the host cell cytosol and consist of chains of M. tuberculosis of a small size.
(A-B) Correlative light electron microscopy (CLEM) images of hLEC infected with M. tuberculosis-GFP. Top left subpanel shows the light microscopy images, with the corresponding electron microscopy images in the top right subpanel. The larger subpanels show a composite of the fluorescence overlaid onto the electron microscopy. (A) M. tuberculosis intracellular cord, without any encapsulating host membrane, indicating that it is present in the cytosol. (B) M. tuberculosis encapsulated in a membranous compartment, as a control for confirming membrane preservation due to the sample preparation. Host cell membrane is highlighted in red. (C-D) To quantify the volume of M. tuberculosis, individual bacteria were manually segmented from slices of SBF SEM images and 3D reconstructions of selected bacteria were made (coloured rods), using 3dmod. Representative reconstructions are shown, with corresponding fluorescence highlighted (matched manually with the corresponding SBF SEM slice in Z, and then aligned in xy with TurboReg in Fiji). Dataset dimensions; (C) Left panel: 8.7 x 8.7 x 50 nm pixels, Right panel: 71.3 x 71.36 x 1 µm in xyz; (D) Left panel: 6.3 x 6.3 x 50 nm pixels; Right panel: 51.6 x 51.6 x 2.75 µm in xyz. (E) The volume of each bacterium reconstruction from two independent sample datasets was calculated in 3dmod, and a comparison between those in a membrane bound compartment and those in an intracellular cord was made. The data ± SEM show that individual bacteria forming cords are significantly smaller. Student's t-test: ** = $p < 0.01$.

Figure 4

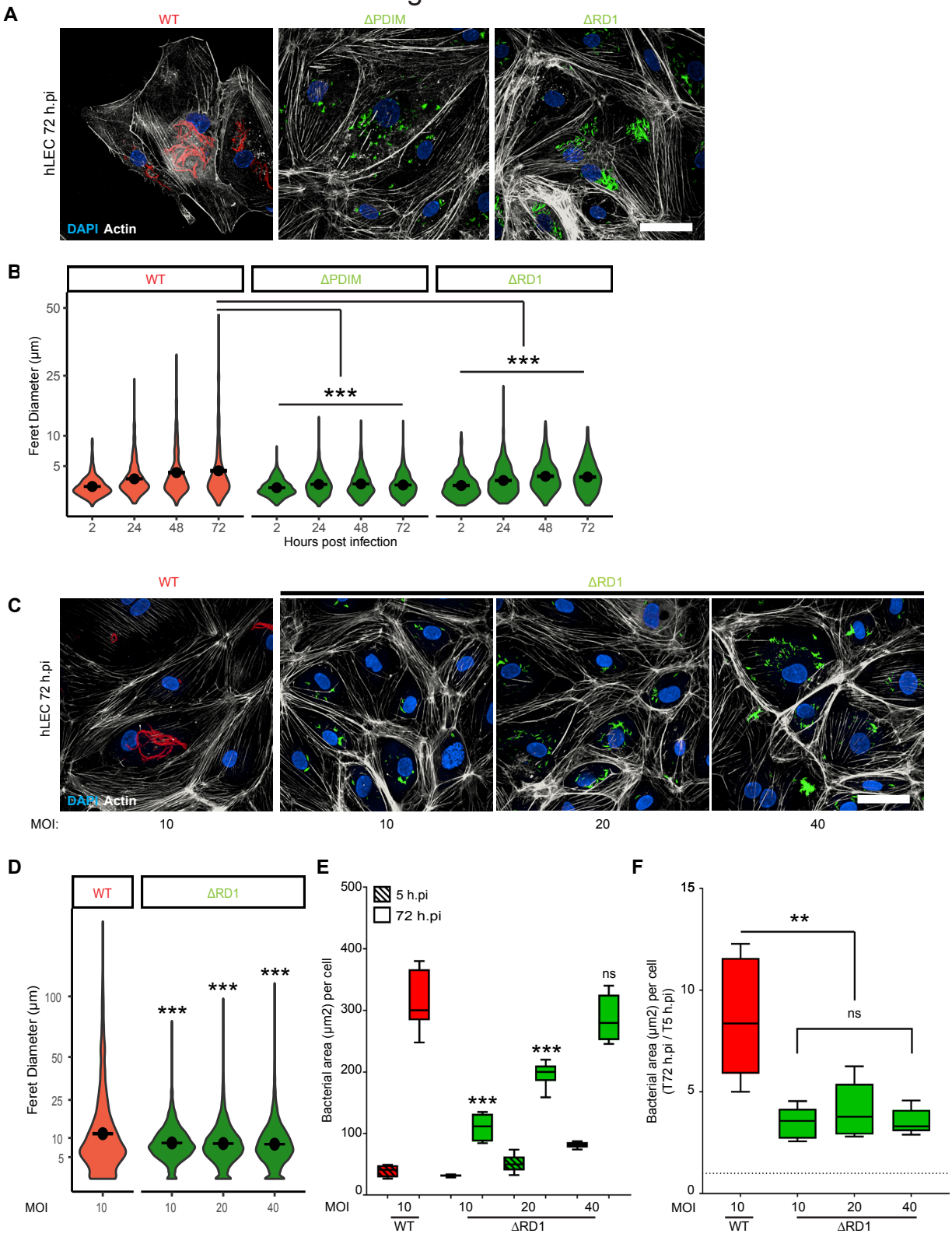

Figure 4: M. tuberculosis lacking RD1 locus or PDIMs expression fail to cord within hLECs

(A) hLEC were infected with RFP-expressing M. tuberculosis WT, GFP-expressing M. tuberculosis ΔPDIM or E2-Crimson-expressing ΔRD1 for 72 h at a MOI of 10, fixed and stained for F-actin with AF633 or AF488-phalloidin. Either deleting PDIM or the RD1 locus abolished cord formation. WT bacteria (red), Δ PDIM and ΔRD1-bacteria (green), F-actin (white) and nuclei (blue). Scale bar is 50 µm. (B) Feret diameter measurements from three independent experiments were plotted. For each condition tested, the number of bacterial clusters analysed is between 600 and 1,200 (C) hLEC were infected for 72 h with RFP-expressing M. tuberculosis WT at a MOI of 10, or with E2-Crimson-expressing M. tuberculosis ΔRD1 at a MOI of 10, 20 or 40. WT bacteria (red), Δ RD1-bacteria (green), F-actin (white) and nuclei (blue). Scale bar is 50 µm. (D) Feret diameter measurements from images in (C) from two independent experiments were plotted. The number of bacterial clusters analysed are: 3,960 for WT and 6,470, 9,472, 11,759 for ΔRD1 at MOI:10, 20 and 40, respectively. (E) Quantification of the bacterial load per cell, expressed in bacterial area (µm2) per cell, following the uptake (5h.pi) and 72h post infection. (F) Intracellular bacterial growth after 72h infection, expressed by the ratio bacterial area per cell 72h.pi/5h.pi. Values > 1 represent the bacterial growth. (E and F) Data ± SEM are representative of two independent experiments performed in duplicate. (B, C, D and E) One-way ANOVA with Tukey's multiple comparisons tests against WT: ** = p<0.01; *** = p <0.001; ns: no significant.

Figure 5

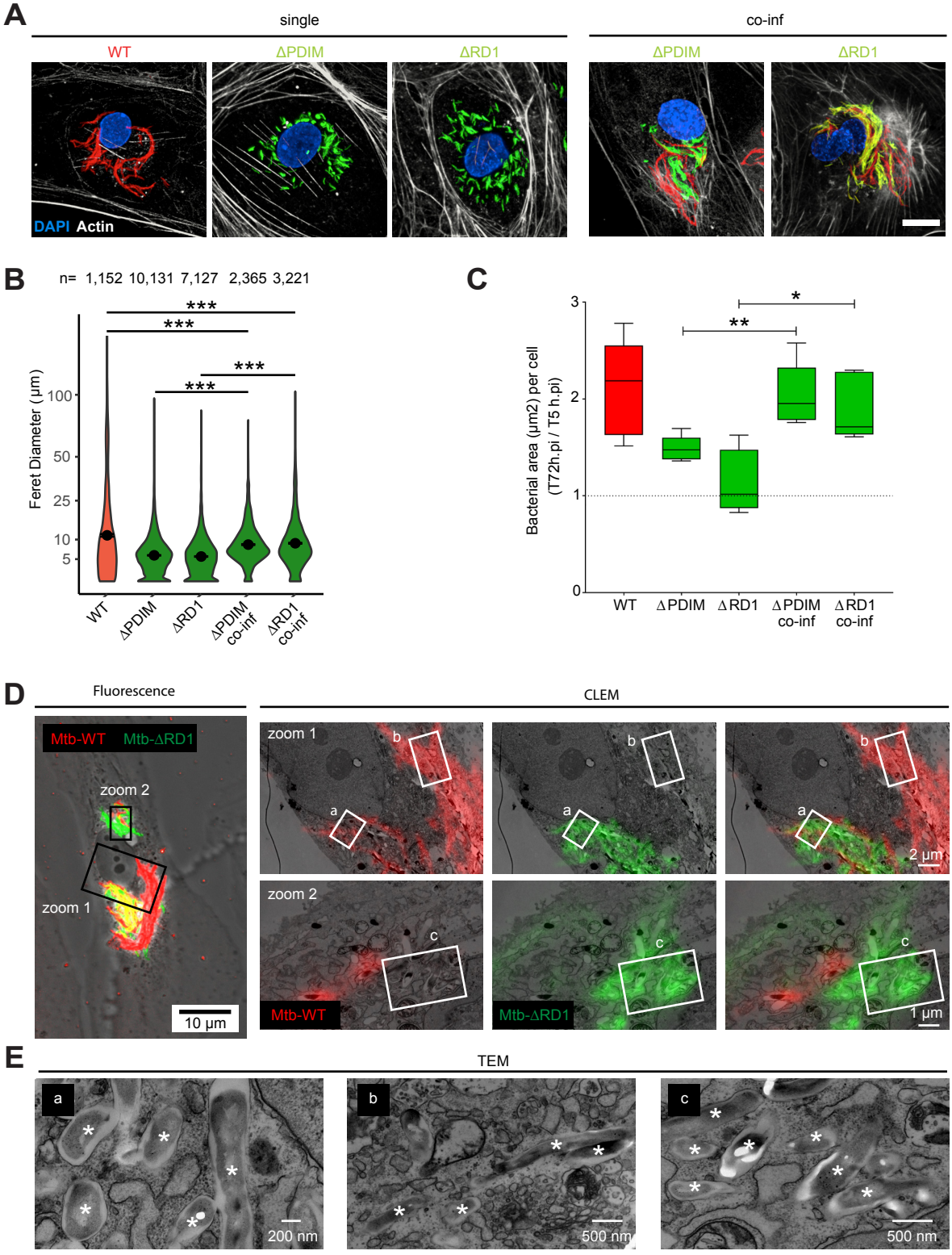

Figure 5: Access to the cytosol is required for M. tuberculosis intracellular cording
(A) hLEC were infected for 72 h with M. tuberculosis WT-RFP (red), M. tuberculosis-ΔPDIM-GFP (green), M. tuberculosis-ΔRD1-E2-Crimson (green) either individually or as a co-infection WT-RFP/ΔPDIM-GFP or WT-RFP/ΔRD1-E2-Crimson. Cells were then fixed and stained for F-actin with AF633 or AF488-phalloidin (Both visualized in white) and DAPI (blue). Scale bar is 10 µm. The images show that during single infection, M. tuberculosis WT exhibits intracellular cording, whereas M. tuberculosis ΔPDIM or ΔRD1 do not. However, in the co-infected sample, both M. tuberculosis ΔPDIM and ΔRD1 were able to form intracellular cords. (B) Feret diameter measurements from images in (A) were plotted. n represent the number of bacterial clusters analysed. (C) Intracellular bacterial growth after 72h infection, expressed by the ratio bacterial area per cell 72h.pi/5h.pi. Values > 1 represent the bacterial growth. (A-C) Data ± SEM are representative of three independent experiments. One-way ANOVA with Tukey's multiple comparisons tests: * = p<0.05; ** = p<0.01; *** = p <0.001. (D-E) Co-infected hLEC samples were processed for correlative light electron microscopy (CLEM) to confirm at the ultrastructural level that M. tuberculosis ΔRD1-GFP cords were indeed present in the cytosol (E; magnifications of regions indicated in D, asterisks mark cytosolic bacteria).

Figure 6

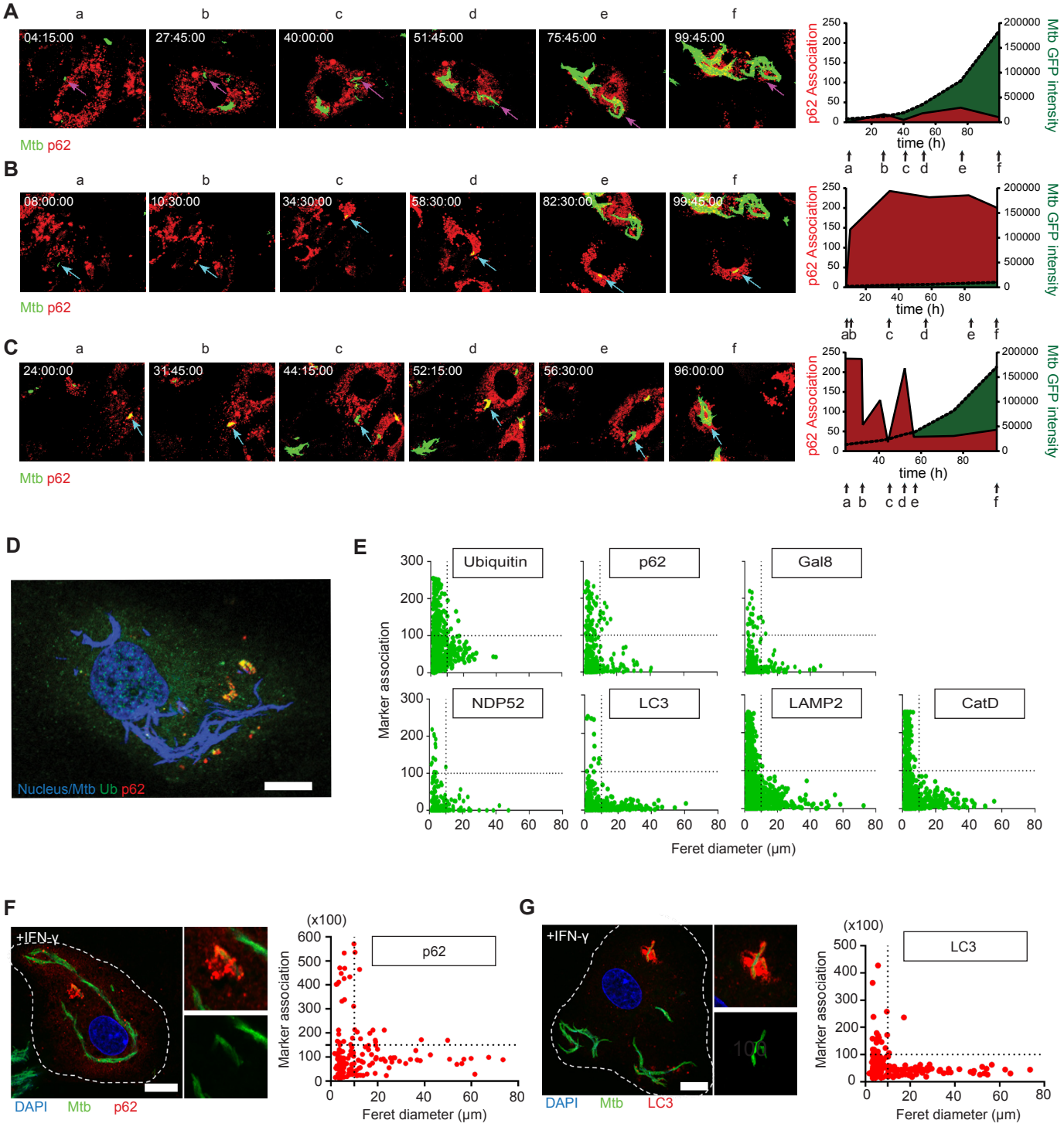

Figure 6: Intracellular cords are not recognized by cytosolic immune sensors in both resting or IFN-γ-activated hLECs.
(A-C) Live cell imaging of hLEC expressing p62-RFP (red) infected with M. tuberculosis-GFP (green) for 115 h. Imaging started 15 min after addition of the bacteria to the cells. Snapshots from the movies (Supplemental Movies 1-3) are shown, with the timepoint displayed above in hh:mm:ss format. Scale bars are 10 µm. (A) The pink arrow tracks an example of an intracellular cord forming from a single bacterium, which never interacts/associates with p62. (B) The blue arrow tracks an example of an individual M. tuberculosis bacterium becoming associated to p62 throughout which leads to restriction of growth. (C) The blue arrow tracks an example of M. tuberculosis associating and dissociating with p62 multiple times. Only after p62 association ceased completely, cord formation started. (c-e, right hand panel) ImageJ quantification of the GFP intensity and the p62-RFP association of the arrowed bacteria over time. Letters a-f refer to the snapshots in (A-C). (D) Representative image of hLEC infected M. tuberculosis WT-EGFP (blue) for 72 h and stained for the autophagy adaptor p62 (red) and the autophagy receptor ubiquitin (Ub) (green). Cell nuclei are stained with DAPI (blue). Scale bar is 10 µm. (E) Intracellular markers of autophagy, pathogen sensing were assessed for their association to intracellular cords 72 h post infection. Particles with a Feret diameter greater than 10 µM were considered cords, and a marker association score above 100 was considered positive. Points correspond to individual bacterial particles. (F and G) Representative image of hLEC infected M. tuberculosis WT-EGFP (green) for 72 h to let bacteria forming intracellular cords before being treated or not with 200 ng/mL of human IFNG for an additional 24 hour. Cell were then fixed and stained for the autophagy adaptor p62 (F, left panel) or LC3 (G, left panel). Both p62 and LC3 markers are visualized in red, cell nuclei are stained with DAPI (blue). Scale bar is 10 µm. Intracellular markers p62 (F, right panel) and LC3 (G, right panel) were assessed for their association to intracellular bacteria in function of the size of the bacterial cluster. Particles with a Feret diameter greater than 10 µM were considered cords, and a marker association score above 15, 000 for p62 and 10, 000 for LC3 were considered positive.
(D-G) Data were obtained from three independent experiments, each performed in duplicate.